The RIB production target for the SPES project

Alberto Monetti[1,2,a], Alberto Andrighetto[1], Carlo Petrovich[3], Mattia Manzolaro[1], Stefano Corradetti[1], Daniele Scarpa[1], Francesco Rossetto[1], Fernando Martinez Dominguez[1,4], Jesus Vasquez[1], Massimo Rossignoli[1], Michele Calderolla[1], Roberto Silingardi[1], Aldo Mozzi[1], Francesca Borgna[1,5], Gianluca Vivian[1], Enrico Boratto[1], Michele Ballan[1], Gianfranco Prete[1], and Giovanni Meneghetti[2]

[1] INFN, Laboratori Nazionali di Legnaro, viale dell'Università 2, 35020 Legnaro (PD), Italy
[2] Department of Industrial Engineering (DII), University of Padua, via Venezia 1 - 35131 Padova, Italy
[3] ENEA, Via M.M. Sole 4, 40129 Bologna, Italy
[4] ESS Bilbao, Instituto de Fusión Nuclear, José Gutiérrez Abascal 2, 28006 Madrid, Spain
[5] Department of Pharmaceutical and Pharmacological Sciences, University of Padua, via Marzolo 5 - 35131 Padova, Italy

Abstract. Facilities making use of the Isotope Separator On-Line (ISOL) method for the production of Radioactive Ion Beams (RIB) attract interest because they can be used for nuclear structure and reaction studies, astrophysics research and interdisciplinary applications. The ISOL technique is based on the fast release of the nuclear reaction products from the chosen target material together with their ionization into short-lived nuclei beams. Within this context, the SPES (Selective Production of Exotic Species) facility is now under construction in Italy at INFN-LNL (Istituto Nazionale di Fisica Nucleare - Laboratori Nazionali di Legnaro). The SPES facility will produce RIBs mainly from n-rich isotopes obtained by a 40 MeV cyclotron proton beam (200 μA) directly impinging on a uranium carbide multi-foil fission target. The aim of this work is to describe and update, from a comprehensive point of view, the most important results obtained by the analysis of the on-line behavior of the SPES production target assembly. In particular an improved target configuration has been studied by comparing different codes and physics models: the thermal analyses and the isotope production are re-evaluated. Then some consequent radioprotection aspects, which are essential for the installation and operation of the facility, are presented.

1 Introduction

Facilities making use of the Isotope Separator On-Line (ISOL) method for the production of Radioactive Ion Beams (RIB) are attracting significant interest in the worldwide nuclear physics community. The ISOL technique is based on the fast release of the nuclear reaction products from the specifically chosen target material together with their ionization into RIBs of short-lived nuclei, to be used for nuclear structure and reaction studies, astrophysics research and interdisciplinary applications.

The SPES (Selective Production of Exotic Species) facility has been designed with the primary goal of producing these intense exotic beams [1,2] and is now under construction in Italy at INFN-LNL (Istituto Nazionale di Fisica Nucleare — Laboratori Nazionali di Legnaro): the radioactive nuclei, mainly n-rich isotopes, will be produced by the fission interactions of a 40 MeV proton beam, at currents up to 200 μA, with an uranium carbide target [3].

This target system will produce a rate of about 10^{13} fissions per second of about 42 different elements.

Many studies have already been performed about the SPES facility, among which [3–6]. The aim of this paper is to update and collect in a comprehensive view the main results obtained in the last years by the project of the target assembly: the overall SPES facility with the description of the general design of the target-ion source assembly will be firstly presented (sect. 2). Secondly, the evaluation of the target isotope productions will be reported according to different release times (sect. 3), as well as the feasibility of the target system with the expected proton beam characteristics (sect. 4). Finally, the preliminary radioprotection aspects for the target assembly are evaluated (sect. 5). All this is performed by means of different simulation codes, such as MCNPX and FLUKA for the interaction of the proton beam with the uranium carbide and the materials surrounding the disks; CINDER90, FISPACT and again FLUKA for activation purposes; ANSYS for the thermal calculations. The use of different codes is motivated by the fact that the accuracy of the computer codes is not

---

high for the considered reactions (fissions induced by 20–40 MeV protons) and the foreseen temperatures of the tar-get disks are not very far from the limiting technological temperatures.

2 The target and ion source unit

The driver for the SPES target is the C70 H$^-$ cyclotron of Best Cyclotron Systems, Inc., a member of TeamBest^{TM}, with maximum current of 0.750 mA and variable energy (30–70 MeV) [2]. In an ISOL facility, the target and the ion source system form a self-contained unit specifically optimized for each element or group of elements. The importance of choosing the specific ion source is primarily dictated by the efficiency optimization and secondarily by its capability of selective ionization. Two standard SPES ion-source types are currently being investigated: the surface ionizing (SSIS) and the plasma ionizing (SPIS) sources. The ions produced with the aforementioned sources are then accelerated towards the ion extraction electrode by a potential up to 40 kV. By means of a series of deflectors and quadrupoles, the beam is then focused after a Wien Filter for a preliminary separation, decreasing as much as possible the contaminants. After a Beam Cooler (BC), which will decrease the longitudinal and transversal emittance, the High-Resolution Mass Separator (HRMS) is foreseen to purify the desired beam from the isobar masses. The beam, if required, can be delivered to the users for low energy experiments. On the other hand, if a high-energy beam is necessary, the selected isotopes will be stopped inside a Charge Breeder (CB) and extracted with an increased charge state (n$^+$). A final mass selector will be installed before reaching the ALPI re-accelerator[7], to clean the beam from the contaminations introduced by the charge breeder itself. The injection to the ALPI Linac will be based on the use of a Radio Frequency Quadrupole (RFQ), with the adiabatic bunching inside. In this way a high-voltage platform can be avoided, and a higher overall transmission efficiency could be achieved. This accelerator assembly will deliver ion beams at energies of 10 A MeV and higher, for masses in the region of $A = 130$ amu, with an expected rate at the user above 10^8 pps.

The Target and the Ion Source (TIS) consist of the production target and the ion source, linked together by means of a tubular transfer line. In order to optimize the 10 kW heat dissipation, the SPES target consists of multiple thin disks housed in a cylindrical graphite box [3]. This configuration, by dissipating efficiently the heating coming from the proton beam, allows higher total beam powers and consequently higher total isotope yields. Moreover, the high fission number is coupled with an expected short release time of the isotopes thanks to the thin disks and to the relative low density of the UC$_x$. The result is a simple, compact and reliable target coupled with components belonging essentially to an already mature technology.

The SPES production target [3], see fig 1, is composed by 7 uranium carbide disks, all characterized by a diameter and a thickness of 40 and 0.8 mm, respectively,
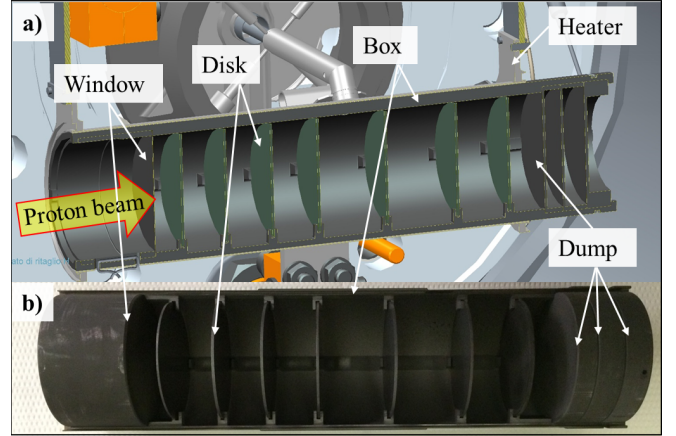

Fig. 1. (a) The SPES production target. (b) Picture of the graphite box containing the disks and both the window and the dumper assemblies. The window and the dumps are not clearly visible due to the shapes of the components.

with a density of about 4 g/cm^3 for the uranium carbide manufactured. The previous study of the disks design [3] had higher thicknesses of the disks due to the lower uranium carbide density assumed there (2.5 g/cm^3). The target heating system consists of a thin tantalum tube, with a length of about 170 mm, an external diameter and a thickness of 50 and 0.2 mm, respectively.

The most common type of uranium carbide produced, tested and used in ISOL facilities is commonly referred to as UC$_x$, indicating that it is composed of different phases: uranium dicarbide (UC$_2$), graphite (C), and a minor amount of uranium monocarbide (UC) [8,9].

In recent years, the synthesis and the characterization of uranium carbide thin disks (SPES target prototypes) have been successfully carried out [4,10], and the production methodology can be considered mature.

The synthesis is based on the reaction between a proper uranium source, typically uranium dioxide, and graphite:

$$UO_2 + 6C \rightarrow UC_2 + 2C + 2CO, \qquad (1)$$
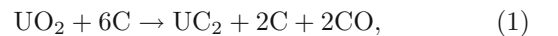
which is made to occur at high temperature (up to 1800 °C) in high vacuum ($\sim 10^{-6}$ mbar).

The production route for the disks to be used as SPES targets consists of the following steps:

– Mixing of the precursors powders by means of an agate mortar or using a planetary ball mill. A small quantity of a phenolic resin binder, usually 2% wt., is used to provide the pressed green pellet with sufficient mechanical stability to be handled without damage and loss of powder.
– Uniaxial cold pressing of the mixed powders into pellets, making use of a hydraulic press and a specifically designed die.
– After extraction of the pressed pellet from the die, its thermal treatment is carried out in a high vacuum furnace specifically developed to reach very high temperatures (~ 2000 °C).
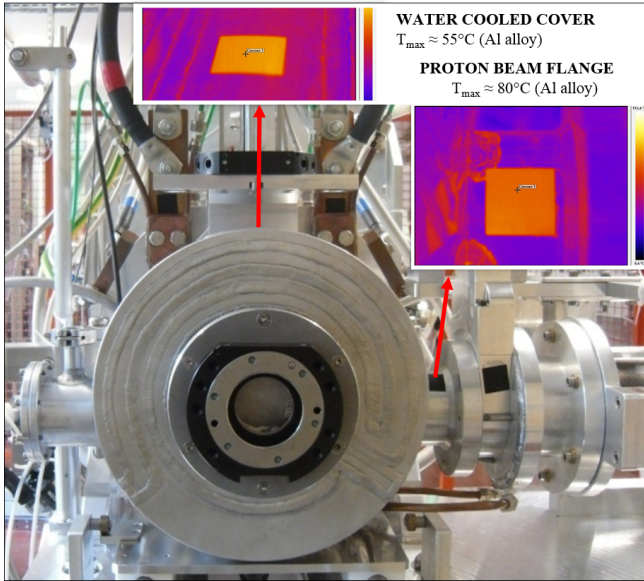
Fig. 2. High power testing, by means of infrared thermography and high emissivity labels, of the target unit chamber containing the SPES TIS system (target and ion source heating power approximately equal to 10 kW and 2 kW, respectively).

The performance of the UC_x target in terms of both isotopes production and thermal stability has been successfully evaluated during two low power irradiation tests at HRIBF facility of the Oak Ridge National Laboratories (ORNL) [4,11]. In these tests, a good correspondence between the electro-thermal simulations and the on-line behavior of the target-ion source system has been obtained [4]. Moreover a SiC target has been tested under high power density conditions (0.5 kW–650 W/cm^3) showing a good structural and thermal stability during the test [12].

The radioactive isotopes produced in the SPES target diffuse inside the target material and then effuse through the transfer line in the direction of the ion source, where they acquire the $1+$ charge state needed for their extraction. The selection of the most appropriate TIS system is of paramount importance since its performance determines the beam intensity, the beam quality, and the number of radioactive beams that can be provided for experimental use. The choice of a specific ion source is primarily dictated by the efficiency, and secondarily by its capability of selective ionization.

The ionization mechanisms that will be implemented in the SPES ion sources are: the surface ionization [13], the laser ionization and the electron impact ionization [5]. They correspond to two different ion sources that define, as a consequence, two different TIS systems.

All the SPES TIS systems presented are placed inside a water-cooled vacuum chamber (target unit), capable to dissipate the amount of power associated to both the target and the ion source, and to guarantee a vacuum level of approximately 10^{-6} mbar [14]. As shown in fig. 2, all the main components of the chamber were accurately monitored by means of infrared thermography and high

emissivity labels. During the test, where the TIS system was heated by 12 kW of DC power, no critical temperatures in the aluminum chamber were evidenced.

3 Production target performances

The goal of the SPES project is the production of radioactive ion beams. Therefore it is essential in the design phase to obtain an estimation of the interactions rates and of the yields of the various isotopes produced in the target. Moreover, this is necessary also to plan the shielding for radioprotection purposes and the SPES facility security. Thus, a more expansive campaign of simulations has been performed by means of the computer codes MCNPX 2.7e [15] and FLUKA v2011-2b [16,17] and their results have been compared, taking into account also that the accuracy of the codes for the production of individual isotope is not high in the considered energy range.

MCNPX and FLUKA are fully integrated Monte Carlo packages for the simulation of the transport and interaction of particles and nuclei with matter. The nuclear interactions generated by ions are treated through interfaces with external event generators since cross-section libraries are not available for all materials, energies and reactions. In FLUKA, the Boltzmann master equations computational theory is implemented in the considered energy range [18]. This is generally used to predict the average multiplicities of particles emitted during the thermalization of an excited nucleus by nucleon-nucleon interaction cascades.

In order to validate the FLUKA results for proton-induced fissions on ^{238}U in the energy range considered, fission yield spectra calculations at 20–60 MeV have been compared with the experimental data reported in [19]. This is achieved simulating beams impinging on a thin target (a thickness of 10 μm has been used, slowing down a 20 MeV proton beam by only 0.2 MeV). The results are shown in fig. 3. FLUKA fission models show a general good agreement, even if the shapes of the curves are narrower than those of the experimental data [19]. Moreover, FLUKA shows a 3-peak shape, especially for energies higher than 50 MeV, not present in the data. Since the SPES project focuses on energies lower than 40 MeV and on nuclei with $80 < A < 160$, FLUKA calculations are here considered as acceptable.

As far as MCNPX is concerned, two models, Bertini [20] and Isabel [21], have been taken into account for the intra-nuclear cascades, while three models, ABLA [22], ORNL (Oak Ridge National Laboratory, [23]) and RAL (Rutherford Appleton Laboratory, [24]), have been considered for the evaporation-fission action. Some of these results were already obtained in [3], but only for MCNPX with Bertini+ORNL and Bertini+RAL and without taking into account the decay chains of the nuclei. ABLA has been used even if its development regarded mainly incident energies higher than 200 MeV [25].

The comparison of the total number of fissions obtained by the different MCNPX models and by the FLUKA code shows some discrepancies, as reported in
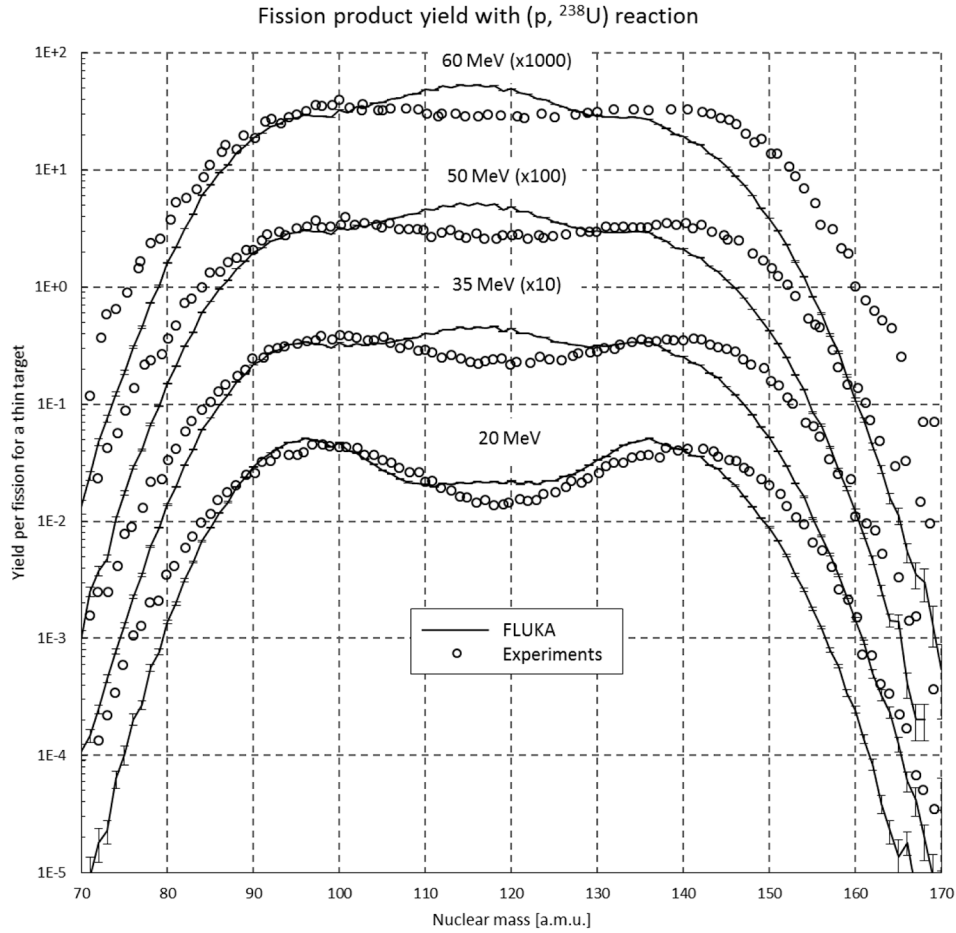
Fig. 3. Comparison of ^{238}U proton-induced fission yields between FLUKA simulations and experimental data reported in [19]. FLUKA Monte Carlo errors are below 2% (except for the external points).

Table 1. Number of fissions per second predicted by the different codes and models (40 MeV, 200 μA).

Model	Fission number [s^{-1}]
Bertini + ABLA	$0.82 \cdot 10^{13}$
Bertini + ORNL	$0.71 \cdot 10^{13}$
Bertini + RAL	$0.73 \cdot 10^{13}$
Isabel + ABLA	$0.82 \cdot 10^{13}$
Isabel + ORNL	$0.71 \cdot 10^{13}$
Isabel + RAL	$0.66 \cdot 10^{13}$
FLUKA	$0.89 \cdot 10^{13}$

table 1. The total average fission rate turns out to be $7.4 \cdot 10^{12}\,\mathrm{s}^{-1}$ for the MCNPX models and the differences with the average value are generally within 10%. FLUKA shows a value 20% higher than the average of the MCNPX ones.

The ^{238}U fission yields by mass number for different nuclear models is reported in fig. 4 and they are mainly in the range between $A = 80$ and $A = 160$, with two peaks at about $A = 100$ and $A = 135$. The differences among the codes are significant and are of the order of a factor of 3 in the center of the curve and up to a factor 1.5 in the two peaks. As expected, the main differences between the curves are due to the different fission models used, while the Bertini and Isabel models provide more comparable trends. The ABLA evaporation/fission model promotes asymmetric fissions stressing the camel production curve, which is only sketched by the RAL model. The model implemented on FLUKA predicts a third peak at about 120 amu. In particular all the results do not predict direct formation of volatile alpha emitters, such as At, Rn and Fr, fundamental inputs for the planning of the vacuum system. The produced isotopes are expected to be on the neutron-rich side of the nuclide chart, with peaks for elements in the unstable regions.

For further evaluations, the FLUKA results have been chosen here due to the fact that even the most reliable model of MCNPX for this energy range (Bertini+ORNL) does not predict the production [3] of expected most neutron-rich nuclei, such as for example ^{133}Sn and ^{134}Sn [26]. The total fission yield in the target is shown in
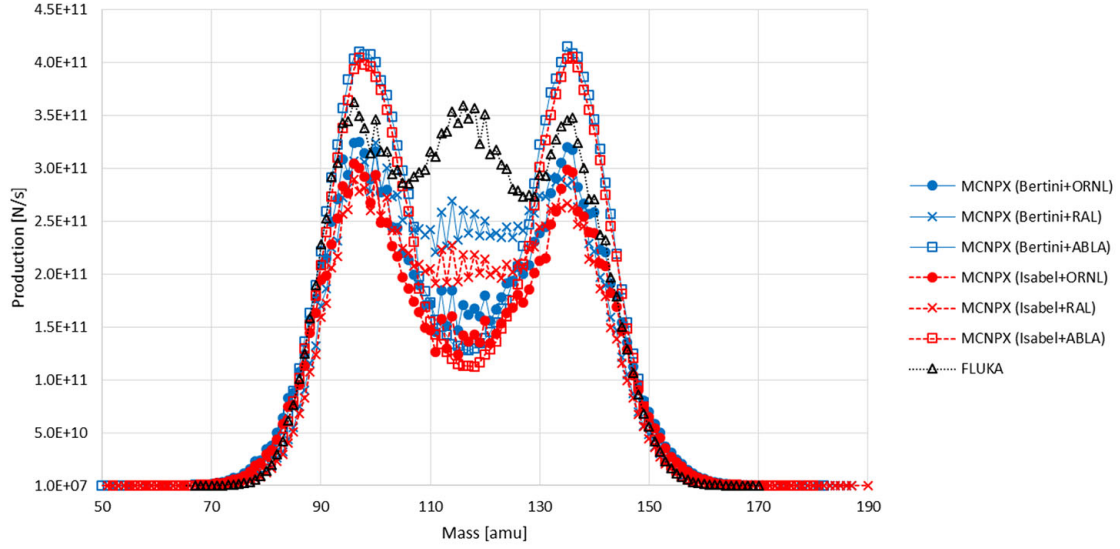
Fig. 4. ^{238}U fission yields by mass number according to different codes and nuclear models (40 MeV, 200 µA).
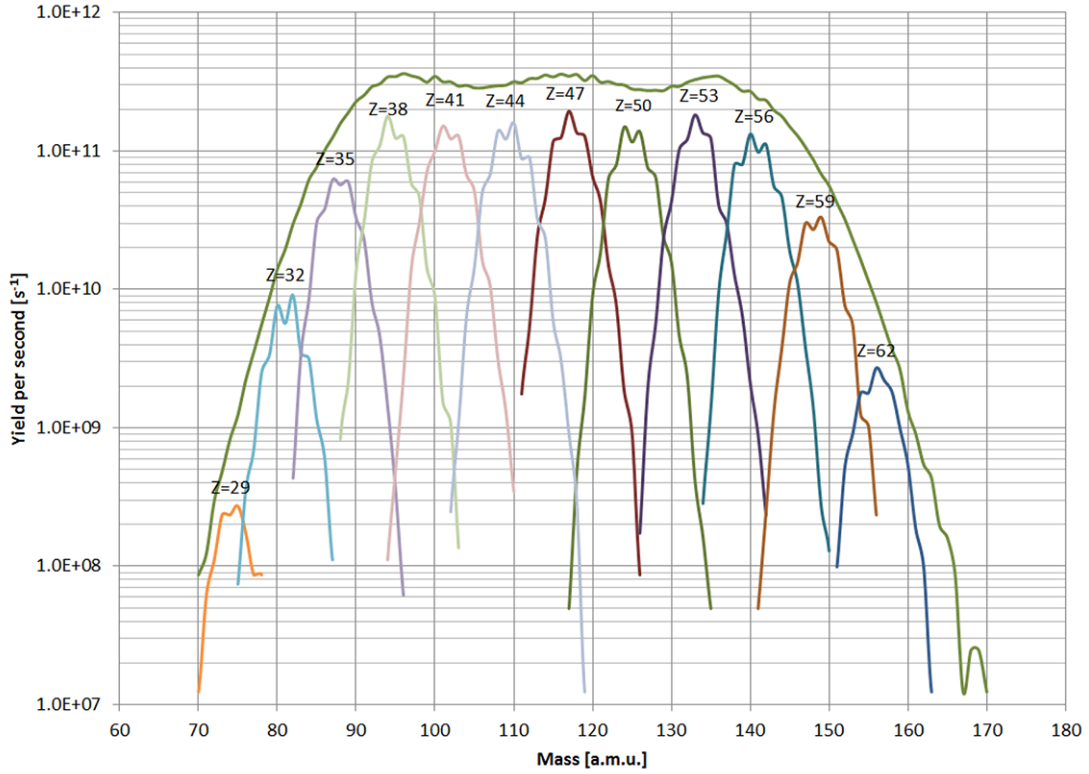

Fig. 5. Formation distribution of some elements in the target (according to FLUKA calculations) together with the total convolution (sum of all the elements). Not all the elements are shown in the figure.

fig. 5, as formed by the sum of all the element contributions, with their typical rough Gaussian distributions.

A very important parameter for the production of RIBs is the release factor, which can be obtained by fitting experimental data with two exponential functions as it is presented in [10, 27]. Since no experimental tests have been implemented yet to evaluate the various coefficients for all the elements, the formula here has been simplified

with one exponential as

$$\varepsilon_r = Be^{-\frac{t}{\tau}},$$

where τ is the isotope half-time, t the release time and B is the constant gathering the diffusion and effusion efficiencies, which are the most critical factors for an efficient release of the exotic atoms from the target to the ion source.
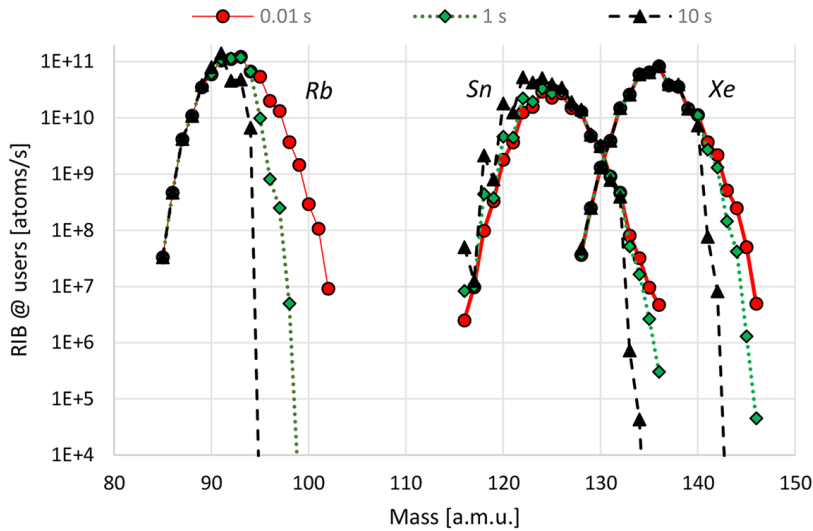
Fig. 6. Production of various elements predicted by FLUKA+decay code. Different release times from the target are considered. Diffusion and effusion efficiencies are not included here ($B = 1$).

These processes are governed by the chemical properties of the various isotopes such as the evaporation temperature and the affinity with carbon and uranium. Most of the isotopes directly produced by the interaction of the proton beam with the uranium nuclei remain trapped and decay in the target ion source system (mainly in the disks), since the short-lived nuclei do not have enough time to reach the ion source and the refractory elements cannot diffuse out for their low vapor pressure (at least without dedicated techniques for the moment not adopted here). A computer code has been implemented to predict the maximum values of isotopes (with $B = 1$) available at the ion source according to different release times. The code takes into account the decay chains of all the isotopes produced, even the most exotic ones. The results of this simulation, following the FLUKA output, evaluate the final beams delivered to the users of the low-energy experiments and are shown in fig. 6. The Rb element is ionized by the Surface Ion Source with efficiency of about 100% [28], Sn by the laser ion source with efficiency 22% [29] and Xe by the plasma ion source with efficiency 47% [30]. Since negligible losses are foreseen along the beam transport line, the overall transport efficiency is conservatively assumed to be 90%.

Using the output from MCNPX with the Bertini + ORNL model, the masses from ^{127}Sn to ^{130}Sn has a higher production rate of about 20–30%, since the expected trend is narrower. It is clear that the release time is the most important factor affecting the production of the shorter half-lives atoms, reducing up to several order of magnitude the intensity of the beam. These simulations are able thus to predict the intensity of the different RIBs, once the target release times and the various yields are better evaluated, and to allow a complete radioprotection analysis. Anyhow, a higher release time increases the production of some nuclei with higher half-life, since they are the decay products of other more exotic nuclei. Further

studies with the RIBO code, already used in [3], will be implemented in order to evaluate the average release time for the various species produced, since it represents the fundamental parameter to characterize the SPES target performances. For example, a higher-energy proton beam leads to higher amounts of exotic yields, but it needs more materials to be stopped (more disks or thicker). The consequence is a higher release time as it was presented in [31] for a 70 MeV target (maximum beam energy deliverable by the purchased cyclotron), leading to a decreasing yield available to the source for the shorter half-lives atoms. Moreover the total atoms available to the source is very sensitive to the release efficiency inasmuch it could vary from almost 100% for high half-live isotopes (100 s) to few percentage points for the short-lived ones (0.1 s).

4 Power deposition calculations and thermal-structural study

Since the foreseen temperatures of the disks are not very far from the upper limits for the UC_x [3], further comparisons have been performed among different computer codes concerning the power deposition in the target.

A flat proton profile had been previously chosen in the analysis of the SPES target, together with a thickness of the disks of about 1.3 mm and a density of 2.5 g/cm^3 [32]. The results obtained with MCNPX, FLUKA and SRIM [33] have been compared below in fig. 7. SRIM is another Monte Carlo code allowing to determine the trajectory and the power deposition by an ion in different materials. The number of protons with SRIM was 0.1% of the particles simulated with the other two codes and this reflects on the more irregular trend compared to the other codes.

Slight differences can be observed for the 1st and 4th disks, due to a different treatment concerning the
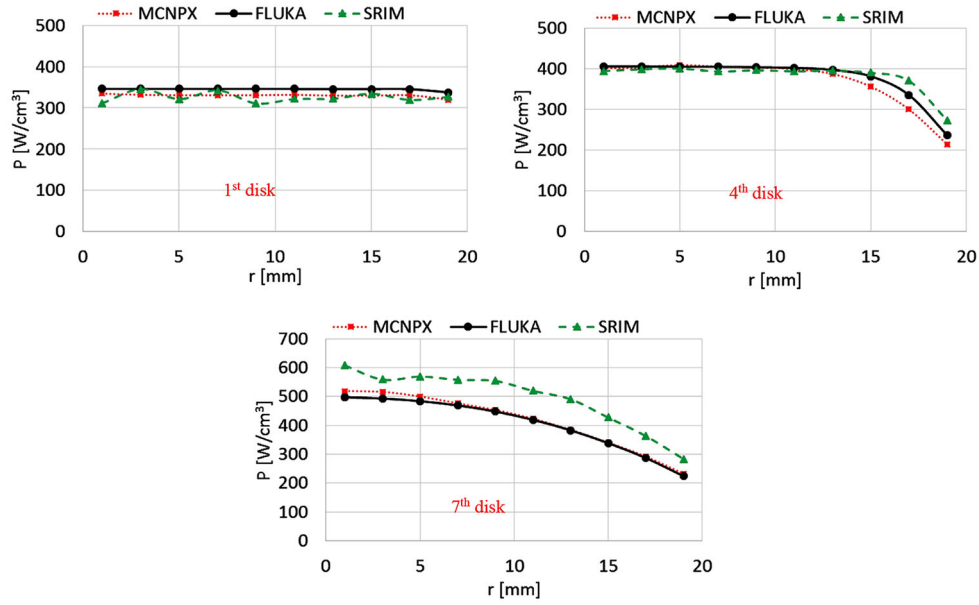
Fig. 7. Power deposition in some UC_x disks (1st, 4th, 7th) of the target according to different Monte Carlo codes.

straggling of the protons by the codes: the highest is in MCNPX, the lowest in SRIM. On the contrary, in the 7th disk, SRIM predicts a power density of about 20% higher. A higher beam straggling has two main effects:

– Higher scattering of protons decreasing the efficiency of the isotopes production.
– Lower power deposition on the last disks.

Therefore the maximum temperatures of a thermal simulation with the results given by SRIM are more conservative than those obtained by FLUKA or MCNPX, which are on the contrary probably the most reliable.

The actual production of the UC_x disks fixes the density of about $4.0\,g/cm^3$, leading to a thickness for all the disks to 0.8 mm. These values are sufficient in order to efficiently utilize the Uranium cross-section since the mean proton energy exiting the last disk is about 15 MeV, leading to a total UC_x mass of 28 g. With respect to the last version of the target [3], a more precise shape of the proton beam produced by the chosen cyclotron has been selected. For a simpler control and, consequently, for safer conditions, the shape of the proton beam has been chosen to be a wobbled Gaussian around the disk axis, with a fixed standard deviation. The wobbler, which allows to rotate the beam, is fundamental to spread the proton beam power along the disk surfaces, as shown in fig. 8, where two different beam profiles have been tested (about 15% of the power is out of the target due to the Gaussian tails). Without wobbling, the power peak in the center of the disk is 50% higher, leading to a substantial increase of the temperature difference between the center and the edge of the disk, with consequent higher stresses. Moreover a smaller proton beam spot, focused on the disks edge thanks to the wobbler, decreases the maximum temperature of the disks in the center and, consequently, decreases the stresses on it.
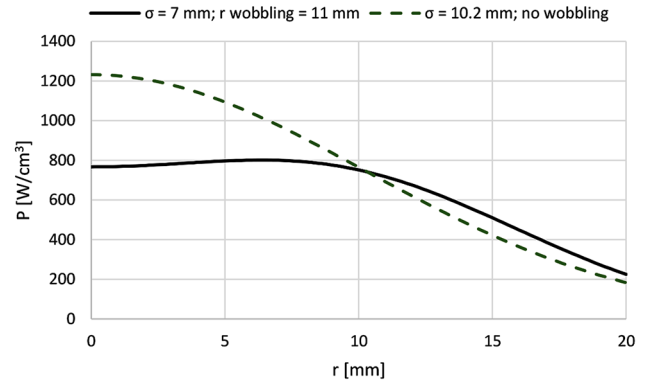

Fig. 8. Power density in the first disk with and without wobbling.

The proton beam properties depend on the emittance of the beam, on the transport lines and on the wobbling system which, as seen previously, strongly influences the reached temperatures. The temperatures of the disks must be kept below 2300 °C, which is the typical melting point of uranium carbide [34–36], and the maximum stresses below 200 MPa [37]. The conductivity has been assumed to be $8\,W\,m^{-1}\,K^{-1}$ [38] and the emissivity 0.85 [8]. A campaign of simulations has been implemented to estimate the new temperatures on the disks with the new boundary conditions. For this purpose, FLUKA has been chosen to simulate the power distribution, considering also the good agreement with MCNPX and with the experimental data shown in the previous analysis. The power deposition has been used as input for ANSYS [39] for the simulation of the target thermal and structural distributions.

An optimum beam has been found with a wobbling radius higher than 11 mm and a standard deviation smaller

Table 2. Power, temperature and highest stresses for the disks in the SPES target impinged by a 40 MeV, 200 μA proton beam.

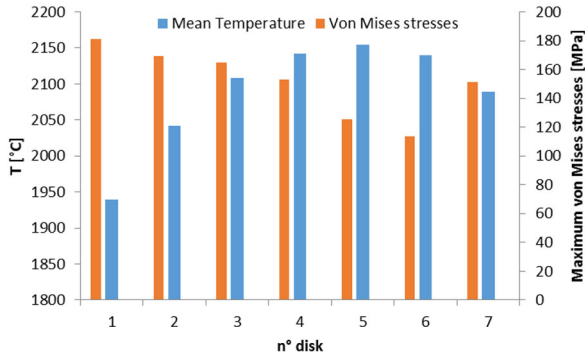| N° disk	P [W]	N_{FISSION} [s^{-1}]	Distance between disks [mm]	T_{mean} [°C]	ΔT_{max} [°C]	T_{max} [°C]	$\sigma_{\mathrm{von\ Mises}}$ [MPa]
1	553	$1.7 \cdot 10^{12}$		2060	174	2127	198
2	572	$1.6 \cdot 10^{12}$	15.5	2169	158	2230	186
3	589	$1.5 \cdot 10^{12}$	16.5	2238	151	2297	181
4	604	$1.4 \cdot 10^{12}$	16.5	2274	139	2330	169
5	597	$1.2 \cdot 10^{12}$	24.5	2288	122	2342	139
6	573	$9.0 \cdot 10^{11}$	25.5	2276	120	2333	125
7	568	$6.3 \cdot 10^{11}$	18.5	2226	160	2299	164

Fig. 9. Mean temperatures and highest stresses for the disks in the SPES target impinged by a 40 MeV, 200 μA proton beam.

Fig. 10. Power density deposited into various disks of the target.

than 7 mm. To remain in conservative conditions, the simulation has been performed with these parameters. A new configuration for the spacing of the disks has been found and the most significant results are presented in table 2 and fig. 9. It is important to underline that the highest stresses are found in the first disks, due to the non-homogenous beam, and the highest temperatures in the central disks (where there is higher power deposition and still not significant proton straggling). The power deposition for some disks is presented in fig. 10. In the first disk it is possible to identify the wobbling effect: the maximum power density is at about 7.5 mm from the center of the disk, but not at the sweeping radius since the area where the beam is spread is wider. The increase of the stopping power at lower energy is observable at the 4th disk, where the power deposition is higher. Moreover the particle straggling moves the power peak towards the center of the disks.

The mean temperatures of the disks are below the temperature limit of 2300 °C (table 2), even if local zones, in the centers of the last disks, still have values (2342 °C) above this limit. A deeper study is under implementation to measure the vapor pressure of the UC$_x$ manufactured for SPES thanks to the Knudsen cell, a fundamental parameter to fix the maximum achievable temperature. Moreover, the maximum sustainable stresses in a high vacuum environment by the actual manufactured UC$_x$ disks will be checked with the same procedure as presented in [40]. Anyhow, if the temperatures turn out
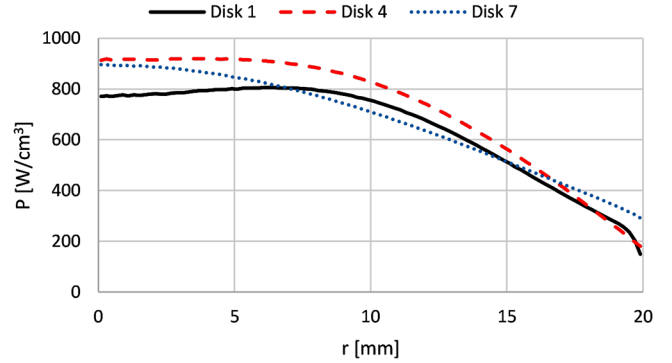
not to be fully sustainable by the disks, a reduction of the beam power of 10% can decrease the temperatures by about 70 °C

A sensitivity study has been implemented to determine the influence of the UC$_x$ conductivity and emissivity in the working conditions. Figure 11 shows that a variation of the 25% of the expected value of the conductivity does not influence the mean temperature of the disks ($\Delta T = 3$–4 °C), whereas the von Mises stresses can change of about 10%. The same considerations were obtained concerning the emissivity: the decrease of about 10% from the assumed value (from 0.85 to 0.75) increases the mean temperature of few degrees (about 10 °C) while it increases the von Mises stresses of about 9%.

The effect of the 50 Hz wobbling beam rotation has been simulated and the time variation of the temperatures at the edges of the target disks has been calculated to be about 2.5 °C, a value considered to be negligible. This is not the case for the stresses since the variation results to be 14 MPa. Moreover an interruption of the wobbler has to be detected as soon as possible (in less than 0.1 s) to avoid excessive temperature increases in punctual zones.

5 Radioprotection calculations

For radioprotection purposes, and in order to design the walls of the bunker in which the SPES front-end will be installed, it is fundamental to evaluate the neutrons emitted
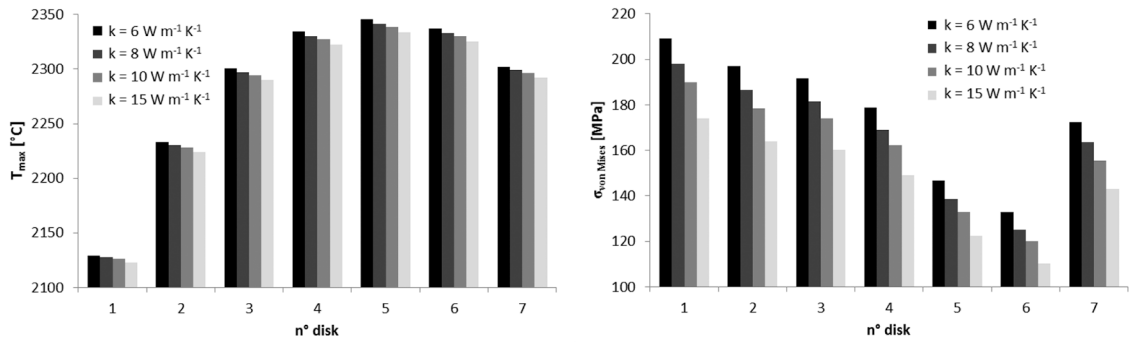
Fig. 11. Variation of the mean temperature and of the maximum von Mises stresses on the disk according to different conductivity.
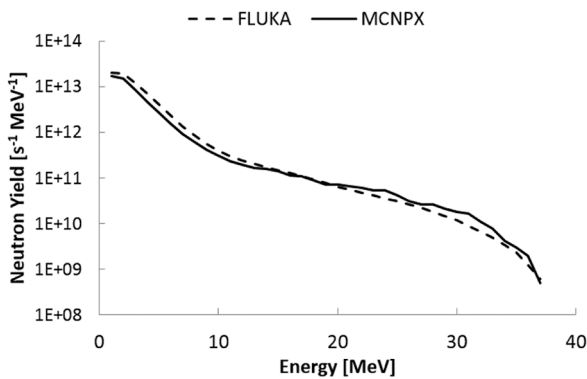

Fig. 12. Comparison of neutron spectrum between FLUKA and MCNPX (Bertini+ORNL) for a 40 MeV, 200 μA proton beam irradiating 28 g of UC$_x$.

by the target. The total number of the neutrons per second foreseen by FLUKA and MCNPX is $7.1 \cdot 10^{13}$ and $5.4 \cdot 10^{13}$, respectively, with a difference of about 30%. The energy spectrum is presented in fig. 12 and similar trends are found for the two codes. The peak is placed for an energy of 1 MeV (typical energies of evaporation-fission neutrons) and after 20 MeV the number of neutrons decreases by about a factor of 100. The higher-energy neutrons are emitted mainly in the direction of the beam, while the lower-energy neutrons are emitted isotropically. Discrepancies are generally within 40% in individual energy intervals and this is here considered acceptable for SPES radioprotection purposes.

This high neutron flux leads to considerable equivalent dose inside the production bunker which is approximately calculated by both codes to be about 2700 Sv/h at 50 cm from the target (see fig. 13).

Another important issue is the estimation of the activity of the irradiated chamber. The target is foreseen to be irradiated by the proton beam for 14 days (reaching about $3 \cdot 10^{13}$ Bq), then to be kept inside the bunker for other 14 days to cool down. After this period, the chamber is placed inside a lead sarcophagus and stored in a dedicated place. To evaluate the activation of the chamber, 3 different codes have been used: CINDER'90 [41], SP-FISPACT [42] (both coupled with MCNPX) and FLUKA.

The results, reported in fig. 14, show a good agreement among the different codes (there is an average discrepancy of 25% for all the values, except for one).

As a preliminary information, after the irradiation period, the cooling time of 14 days decreases the equivalent dose of a factor 100, but the dose remains very high: about 40 mSv/h at 1 m from the chamber. Moreover this calculation does not take into account the activation of all the devices inside the bunker. This level does not respect the maximum dose rate for ordinary maintenance which has been fixed by the SPES safety group at 5 mSv/h. Moreover to enter into the bunker, remove and place the chamber inside a 700 kg sarcophagus, it occurs about 5 min ($\sim$ 3 mSv); then the transport of the sarcophagus until a dedicated repository takes another 5 min (1 mSv), for a total dose of about 4 mSv for one operator every month. A detailed remote target handling system has been designed to solve these issue but its description is out of the scope of this paper.

6 Conclusions

The facilities producing RIBs allow forefront research in the nuclear field, but they also need complex studies of many components and devices that are to be innovatively designed in order to work in an efficient and safe way. The innovative geometry of the SPES target design is able to efficiently produce RIBs thanks to the high yields of the more neutron rich species and an expected short release time from the disks.

An overview of the state-of-the-art studies accomplished in the last years for the SPES target has been presented here. Firstly the SPES facility layout has been described with all its main components. The choice of the cyclotron as primary driver lead to a defined beam shape and a consequent upgrade of the target configuration (mainly in the geometry, the materials and the wobbling beam) with respect to previous papers. These improvements did not worsen the target performances both from an isotope production point of view (influenced by the fission rate) and a safety point of view.

Since the simulations show that the nominal temperatures of the target are not very far from the UC$_x$ limiting
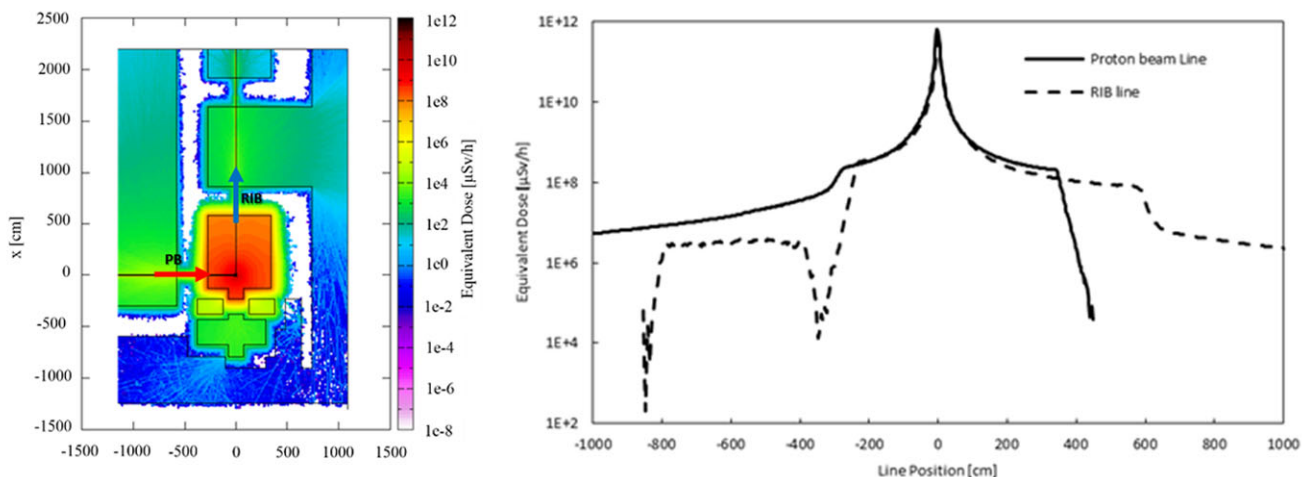
Fig. 13. Equivalent dose due to the neutron flux calculated by FLUKA in the areas close to the bunker (PB - Proton Beam, RIB – Radioactive Ion Beam).
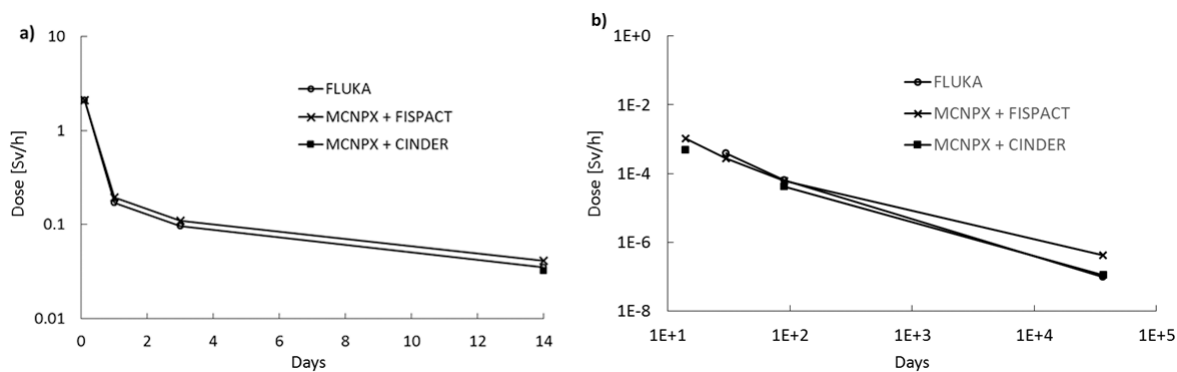

Fig. 14. (a) Total gamma dose at 1 m from the chamber after 14 days of irradiation. (b) Total gamma dose at 2 m from the chamber inside the sarcophagus after 14 days of irradiation. Calculations are performed for a 40 MeV, 200 μA proton beam.

technological temperatures and since the accuracy of the computer codes is not high for the considered reactions (fissions induced by 20–40 MeV protons), a comparison of the results obtained by different computer codes has been considered appropriate.

The evaluation by some of the most reliable Monte Carlo codes, such as MCNPX and FLUKA, showed a good agreement or, in some cases, discrepancies that are considered acceptable for the purposes of the SPES facility.

The behavior of the target under the foreseen proton beam has been fully characterized both with thermal and structural analyses so that the security of the most problematic points of the overall facility has been shown. The highest temperature has been located on the central disks whereas the highest stresses on the first one, due to the non-uniform shape of the proton beam.

Finally, the studies concerning the material activation and the radioprotection of the target were reported. These lead to the design of a remote controlled system to handle the chamber and to couple it with the front-end.

The construction of the whole infrastructures, including the cyclotron, is planned to be realized within 2015. It is foreseen to fully operate in 2017, whereas the first neutron rich beams produced by the UC_x with 5 μA, 40 MeV

proton beam will be accelerated within 2018. Finally, the nominal proton beam power will be delivered in 2020.

Further R&D studies are being conducted by the SPES target group to test the systems, upgrade the front-end, the Wien Filter and to improve the target-ion source system both from a safety and a functioning point of view. In particular the most important developments are focused on the improvement of a fast maintenance, of a more accurate characterization of the properties of the manufactured UC_x and on the selectivity of the sources to supply to the user purer beams.

References

1. A. Andrighetto *et al.*, AIP Conf. Proc. **1491**, 58 (2012).
2. G. Prete *et al.*, Phys. Proc. **26**, 274 (2012).
3. A. Andrighetto *et al.*, Eur. Phys. J. A **30**, 591 (2006).
4. D. Scarpa *et al.*, Eur. Phys. J. A **47**, 32 (2011).
5. M. Manzolaro *et al.*, Rev. Sci. Instrum. **83**, 02A907 (2012).
6. J. Montano *et al.*, Nucl. Instrum. Methods A **648**, 238 (2011).
7. G. Bisoffi *et al.*, in *Proceedings of HIAT 2012* (Chicago, IL USA, 2012).

8. L. Biasetto *et al.*, J. Nucl. Mater. **404**, 68 (2010).
9. L. Biasetto *et al.*, Eur. Phys. J. A **42**, 517 (2009).
10. S. Corradetti *et al.*, Eur. Phys. J. A **49**, 56 (2013).
11. S. Corradetti *et al.*, Eur. Phys. J. A **47**, 119 (2011).
12. M. Barbui *et al.*, Nucl. Instrum. Methods B **266**, 4289 (2008).
13. M. Manzolaro *et al.*, Nucl. Instrum. Methods B **317**, 446 (2013).
14. M. Manzolaro, *Engineering of the INFN SPES target – ion source system* (LAP Lambert Academic Publishing, 2012).
15. J.S. Hendricks *et al.*, *MCNPX Version 2.5.e*, LA-UR-04-0569 (2004).
16. A. Fassò *et al.*, *FLUKA: a multi-particle transport code*, CERN-2005-10 (2005), INFN/TC05/11, SLAC-R-773.
17. G. Battistoni *et al.*, AIP Conf. Proc. **896**, 31 (2007).
18. M. Cavinato *et al.*, Phys. Lett. B **382**, 1 (1996).
19. V.A. Rubchenya *et al.*, Nucl. Instrum. Methods A **463**, 653 (2001).
20. H.W. Bertini, Phys. Rev. **131**, 1801 (1963).
21. Y. Yariv, Z. Fraenkel, Phys. Rev. C **20**, 2227 (1979).
22. A.R. Junghans *et al.*, Nucl. Phys. A **629**, 635 (1998).
23. J. Barish *et al.*, *HETFIS High-Energy Nucleon-Meson Transport Code with Fission*, ORNL-TM-7882 report (Oak Ridge National Laboratory, 1981).
24. F. Atchison, *Spallation and Fission in Heavy Metal Nuclei under Medium Energy Proton Bombardment*, in *Targets for Neutron Beam Spallation Sources*, Jul-Conf-34, Kernforschungsanlage Julich GmbH (1980).
25. D.B. Pelowitz *et al.*, *MCNPX 2.7.E Extension*, Technical Report LA-UR-11-01502, Los Alamos (2011).
26. J.R. Beene *et al.*, J. Phys. G: Nucl. Part. Phys. **38**, 024002 (2011).
27. A.E. Barzakh *et al.*, Nucl. Instrum. Methods B **126**, 150 (1997).
28. N. Sato *et al.*, Rev. Sci. Instrum. **84**, 023304 (2013).
29. Y. Liu *et al.*, Nucl. Instrumen. Methods B **243**, 442 (2006).
30. L. Penescu *et al.*, Rev. Sci. Instrum. **81**, 02A906 (2010).
31. K. Tshoo *et al.*, EPJ Web of Conferences **66**, 11016 (2014).
32. A. Andrighetto *et al.*, Eur. Phys. J. A **25**, 41 (2005).
33. J.F. Ziegler, M.D. Ziegler, J.P. Biersack, *SRIM The Stopping and Range of Ions in Matter* (2008).
34. M.G. Saint-Laurent *et al.*, *Spiral Phase-II Final Report* (European RTT, 2001).
35. L.C. Carraz *et al.*, Nucl. Instrum. Methods **158**, 69 (1979).
36. S. McLain, J.H. Martens (Editors), *Reactor Handbook* (Interscience Publishers, New York, 1964).
37. Hj. Matzke, *Science of Advanced LMFBR Fuels* (North Holland, Amsterdam, 1980).
38. J.P. Greene *et al.*, Nucl. Instrum. Methods B **241**, 986 (2005).
39. *ANSYS® Academic Research, Release 15.0*.
40. M. Manzolaro *et al.*, Rev. Sci. Instrum. **84**, 054902 (2013).
41. W.B. Wilson, T.R. England, *A Manual for CINDER'90 Version C00D and Associated Codes and Data*, LA-UR-00-Draft (2001).
42. C. Petrovich, *SP-FISPACT2001 A Computer Code for Activation and Decay Calculations for Intermediate Energies. A Connection of FISPACT with MCNPX*, RT/ERG/2001/10 (ENEA, Bologna, 2001).